AMERICAN SCIENTIFIC PUBLISHERS

Science of Advanced Materials
Vol. 7, pp. 1–7, 2015
(www.aspbs.com/sam)

ARTICLE

Synthesis of Ga_2O_3 Nanorods with Ultra-Sharp Tips for High-Performance Field Emission Devices

Yavuz Bayam[1,2], V. J. Logeeswaran[1], Aaron M. Katzenmeyer[1], Ramin Banan Sadeghian[1], Rebecca J. Chacon[1], Michael C. Wong[1], Charles E. Hunt[1], Kenichi Motomiya[3], Balachandran Jeyadevan[3,4], and M. Saif Islam[1,*]

[1]*Department of Electrical and Computer Engineering, University of California at Davis, Davis, CA 95616, USA*
[2]*Department of Electrical and Electronics Engineering, Gediz University, 35660 Izmir, Turkey*
[3]*Graduate School of Environmental Studies, Tohoku University, Japan*
[4]*Department of Materials Science, The University of Shiga Prefecture, 2500 Hassaka, Hikone, Shiga 522-8533, Japan*

ABSTRACT

We synthesized catalyst-free β-Ga_2O_3 nanorods with terminated ultra-sharp tips by heat treating single crystalline GaAs in a chemical vapor deposition (CVD) chamber without introducing a precursor. The unique, straight-forward, synthetic route and a possible growth mechanism are discussed to explain the different morphology of the grown nanorods and the ultra-sharp nanostructures. The morphology and structure of the nanorods were characterized by scanning electron microscopy (SEM), energy dispersive X-ray spectroscopy (EDS), X-ray diffraction (XRD) and Raman-spectroscopy. The ultra-sharp tips were found to have radii of ~3–5 nm and were utilized to achieve enhanced field emission. The field emission characteristics demonstrated a turn-on field of 2.1 Vμm^{-1}, a threshold electric field of 5.6 Vμm^{-1}, and a geometrical field enhancement factor of 3786, making them comparable to nanostructured diamond and highly oriented single wall carbon nanotubes.

KEYWORDS: Gallium Oxide, Nanorod, Field Emission, Field Enhancement Factor.

1. INTRODUCTION

Recently, numerous vertically-oriented one-dimensional nanostructures fabrication methods, using bottom-up synthesis processes have attracted interest owing to their simplicity of synthesis and high electromechanical performance. Materials such as carbon nanotubes (CNTs),[1] wide band-gap semiconductors,[2] metal nanowires[3] and several oxides such as In_2O_3,[4] ZnO,[5] SnO_2[6] and Ga_2O_3[7,8] have stimulated considerable interest. Some of these materials have low work function and/or high chemical stability. Monoclinic gallium oxide (β-Ga_2O_3) is an important transparent metal oxide semiconductor with a wide band gap ($E_g = 4.9$ eV). The electrical conduction[9] and luminescence[10] properties make it a good candidate for optoelectronic applications such as flat panel displays, solar energy devices, and stable high temperature gas sensors.[11] Various methods have been used to synthesize β-Ga_2O_3 nanostructures including thermal evaporation,[12] arc-discharge,[13] laser ablation,[14] and carbothermal reduction.[15]

Field emission (FE), a very well understood quantum mechanical electron tunneling effect, is a good source for high-brightness electrons with low energy spread. Under high electric field strengths, energy barrier thinning enables electrons to escape from the cathode by tunneling through an insulating medium such as vacuum. For many applications using FE, the materials should exhibit very low-field onset of emission and a high degree of stability at high current density. A low work-function and a large field enhancement factor contribute to a low threshold field for electron emission. While work-function is an intrinsic material property, the field enhancement factor (FEF) predominantly depends on the geometry of the emitters. The high aspect ratio and small radii of sharp tip can generate a high local electric field at the tip, which results in a decrease of the FE potential barrier and increase of the FE current.[16] Tedious and costly top-down processing techniques have been demonstrated to fabricate field emission tips with diminishingly small radii,[17,18] although most such emitters have finite lifetime and exhibit performance degradation over a short period of time. Zhan et al. reported the first field emission properties of Ga_2O_3–C nanocables with a turn on field of 7.73 Vμm^{-1}.[19] Recently Cao et al. reported cactus-like gallium oxide nanostructures with a

*Author to whom correspondence should be addressed.
Email:
Received: xx Xxxx xxxx
Accepted: xx Xxxx xxxx

turn on field of 12.6 Vμm^{-1} [15] and Huang et al. reported quasi-aligned Ga_2O_3 nanowires with a turn on field of 6.2 Vμm^{-1}.[20]

In this paper, we report on the synthesis and characterization of β-Ga_2O_3 nanorods with ultra-sharp tips with radii of ~3–5 nm, by directly heating a GaAs wafer in a horizontal tube furnace. A growth mechanism suggested to explain the different morphologies observed on the growth substrate and on the grown ultra-sharp nanostructures. The structures exhibited excellent field emission characteristics with a turn-on field of 2.1 Vμm^{-1} and a threshold electric field of 5.6 Vμm^{-1}. A high value of 3786 was obtained for the overall field enhancement factor using a modified version of the Fowler-Nordheim equation for semiconductor surfaces.

2. EXPERIMENTAL PROCEDURE

The Ga_2O_3 nanorods with ultra-sharp tips were grown in a horizontal alumina tube inserted in a furnace as shown in Figure 1. The tube was continuously pumped down to 749 Torr. Argon was used as carrier gas at a flow rate of 100 sccm, while the residual O_2 in the alumina tube acted as the reaction gas. The Zn-doped *p*-GaAs (100) substrate was first put in a small container filled with deionized water then placed in a ultrasonic bath and cleaned for 4 minutes. After the cleaning process substrate was dried by Nitrogen and then placed in an alumina boat. The boat was placed at a distance of ~12 cm from the center of the alumina tube facing downstream to the flow of carrier gas. The temperature distribution along the tube is not uniform during the heating process. To determine the temperature profile of the tube, a type *K* thermocouple was used. The temperature is the highest at the center of the tube and is ~800 °C where the substrates are located. Prior to heating the tube, Argon was introduced into the system to flush out the tube for ~20 min. Then the furnace temperature was ramped up to 1050 °C from room temperature with a rate of 7 °C/min and was fixed at that value for 40 minutes. Subsequent to this process, the furnace was cooled down to room temperature. Upon retrieving the sample, a layer of white wool-like film was observed on the surface of GaAs substrate.

3. RESULTS AND DISCUSSION

The resulting film was characterized using scanning electron microscopy (SEM), Raman spectroscopy and energy dispersive X-ray spectroscopy (EDS).

For surface morphology characterization, an FEI XL30-SFEG scanning electron microscope (SEM) was employed. The SEM images reveal Ga_2O_3 nanorods (length ~5–15 μm and thickness ~200 nm to 1 μm) densely grown on the substrate and most of them have ultra-sharp tips on the top facet with a large aspect ratio. Figures 2(a) and (b) show the global view of the nanorods while 2(c) shows the cross-sectional SEM micrograph of the Ga_2O_3 nanorods with clearly visible ultra-sharp tips. Figure 2(d) shows truncated pyramidal regions between the nanorods and the ultra-sharp tips. This shape represents the incremental growth from the initial Ga droplet size to the most favorable dimensions for Ga_2O_3 crystal growth in a competitive environment. Figure 2(e) presents a transmission electron microscopy (TEM) image of a nanoscale tip that is visibly decorated with an ensemble of nano-droplets.

The Raman spectra of Ga_2O_3 nanorods were acquired using a Renishaw RM1000 Research Laser Raman Microscope. Figure 3(a) presents the room temperature Raman scattering spectra of Ga_2O_3 nanorods under the excitation wavelength of 514 nm. Raman peaks were obtained at 191, 310, 337, 406, 466, 621 and 646 cm^{-1}. These peaks precisely match with that of single crystalline β-Ga_2O_3.[13, 21]

The chemical composition of Ga_2O_3 nanorods was studied using an Energy Dispersive X-ray Spectroscopy (EDS) module attached to the SEM. The resulting spectrum is shown in Figure 3(b). The EDS data reveal the presence of gallium and oxygen as the main composition of the nanorods, while the arsenic signal is from the substrate. When GaAs is heated above the decomposition temperatures range (585 °C–750 °C), it is brought into the phase separation regime (Fig. 4(b)).[22] In this regime, liquid gallium clusters on the surface are the thermodynamically favored state. Around the decomposition temperature, the lattice structure begins to break down and preferential loss of arsenic (As) occurs from the GaAs surface. Nucleation of clusters and phase separation takes

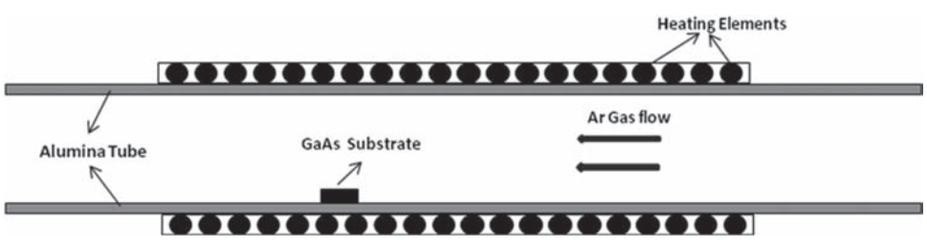

Fig. 1. Schematic illustration of experimental setup consisting of an alumina tube furnace with a precision control heater. Argon flow was used to flush out the tube. The tube temperature was increased to 1050 °C maintaining a growth temperature of ~800 °C around the GaAs growth substrates for synthesizing ultra-sharp Ga_2O_3 nanorods.

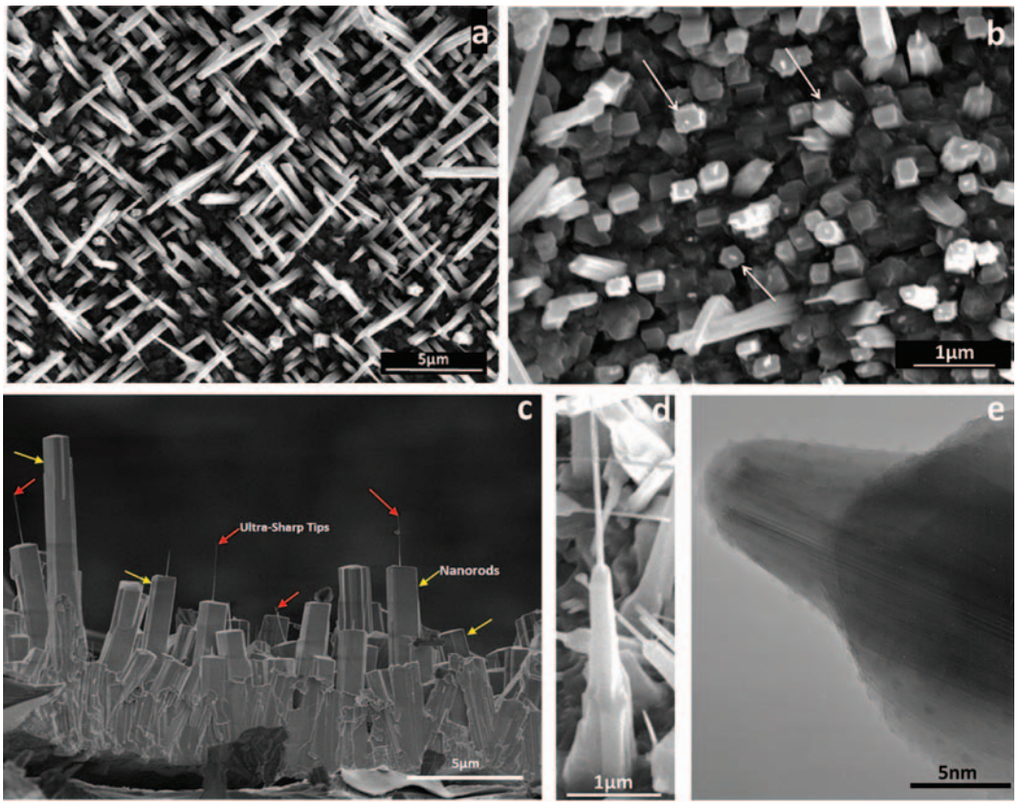

Fig. 2. (a)–(b) Low magnification and (c) high magnification SEM images of Ga_2O_3 nanorods with ultra-sharp tips (indicated with arrows). (d) Truncated pyramidal regions between the pillars and the ultra-sharp tips. (e) Transmission electron microscopy (TEM) image of the sharp tip. An ensemble of Ga or Ga_xO droplets is visible on the tip.

place once sufficient Ga concentration has been reached on the surface.[22] During the cluster formation there are three steps:

(i) arsenic diffusion and evaporation,

(ii) formation of Ga clusters on the surface and desorption of exposed As from the surface, and

(iii) arsenic diffusion and evaporation through the liquid Ga cluster.

Thermodynamic studies of Ga on GaAs show that arsenic loss through liquid Ga is faster than arsenic diffusion through the substrate followed by desorption from the wafer surface.[23]

The diameter of these droplets, found experimentally by Zinke-Allmang et al. to be due to coalescence, corresponds well to the lateral dimensions of the nanorods on which ultra-sharp tips grow.[24] The droplets adopt a hemispherical-type conformation[25] as a result of liquid Ga being able to wet the dynamic GaAs surface; this is due to the strong binding energy towards As.[26] If oxygen concentration is high in the ambient, it is likely that a thick Ga_2O_3 film or micro-columns, instead of nanorods, nanoblocks or nanowires, will form at high temperature ranges (Fig. 4(c)). This means that high oxygen concentration at high temperature inhibits nanoscale structure (nanowires, nanoblocks or nanoribbons etc.) growth (Fig. 4(d)).

Tersoff et al. previously noted that in the absence of oxygen in the chamber, Ga droplets with $\sim \mu$m diameters exhibit a dynamic motion in some preferential directions on the GaAs wafer surface[27] (Fig. 4(d)). A chemical reaction between the residual oxygen gas in the chamber and Ga clusters accumulated on the surface of GaAs substrate takes place. This reaction results in a thin film of Ga_2O_3 with visible voids under it. These voids are due to excess loss of As from hundreds of atomic layers of GaAs (Fig. 5) which were observed before.[28] Beyond the evolution of droplet formation, we note that the formation of a stable Ga_2O_3 film will serve to limit the availability of the Ga species from the substrate to the outermost growth surface (Fig. 4(d)). These considerations for Ga on Ga_2O_3 and the equation of state along with Young's equation suggest a non-wetting contact angle.[29] With this in mind, a bidirectional growth mechanism is proposed for the rather homogeneous ultra-sharp tips on the nano/micro pillars.

The presence of oxygen species enables a Ga_2O_3 "crust"[29] to form which serves to divide the growth into two regimes: that below the film (oxygen diffuses from the surface) and that above it, which explains the one-dimensionality of the ultra-sharp tip. Below this Ga_2O_3

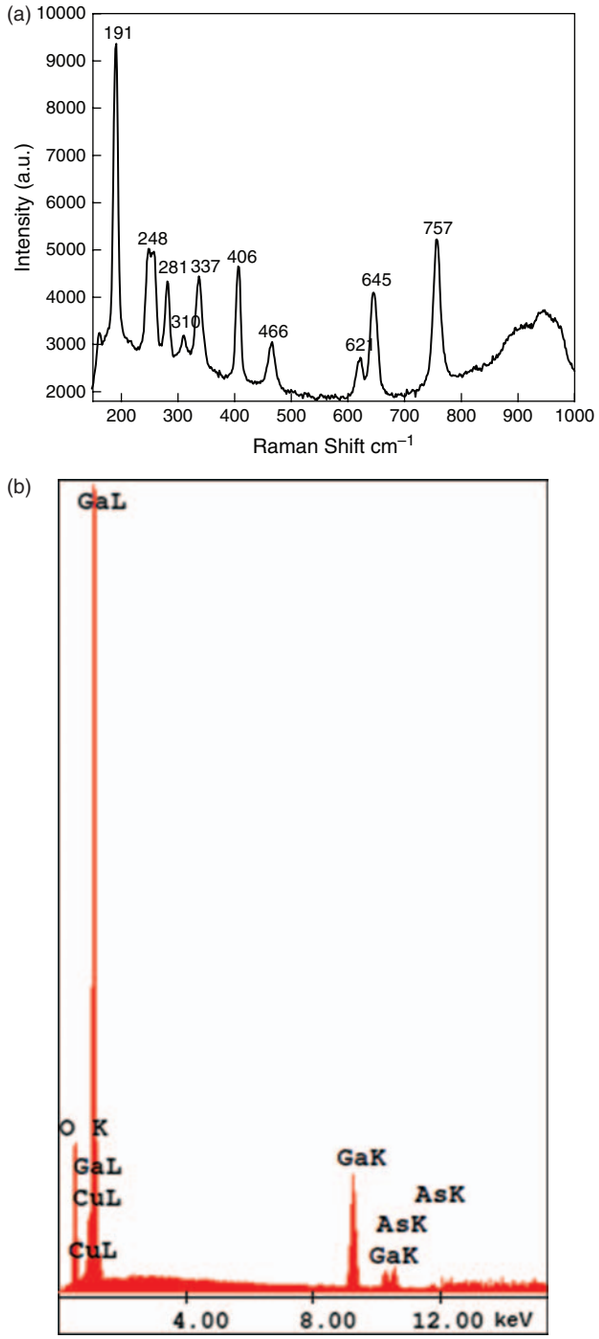

Fig. 3. (a) The Raman spectra of Ga_2O_3 nanorods. The peaks are obtained at 191, 310, 337, 406, 466, 621, 646 cm^{-1}. These peaks match with the literature-reported single crystalline β-Ga_2O_3 Raman peaks and provide further experimental evidence that the as-grown nanorods are single-crystal monoclinic β-Ga_2O_3. (b) EDS measurement of Ga_2O_3 nanorods show that the main composition of the nanorods is Ga and O_2 whereas the As signal is traceable to the substrate.

film, an interfacial liquid Ga layer simultaneously accumulates and wets the GaAs substrate underneath, facilitating continuous downward conversion of the GaAs substrate into Ga_2O_3. Crystal formation and competition from surrounding pillars results in well-defined, constant-diameter pillars. The truncated pyramidal region between the pillars and the ultra-sharp tips represents the incremental growth from the initial Ga droplet size to the most favorable dimensions for Ga_2O_3 crystal growth in a competitive environment (Fig. 2(d)). The ultra-sharp tips are explained by the inability of Ga to wet Ga_2O_3. As the film of Ga_2O_3 forms at the initial GaAs interface, the liquid Ga above the film can no longer wet the surface and equidistantly progresses towards a large contact angle droplet. This inability of the droplet to wet the surface results in the necessity of one-dimensional growth and the volume of the droplet determines the length and subtle tapering of the ultra-sharp, one-dimensional tip. The growth self-terminates with the exhaustion of Ga and may be applicable towards nano-atomic transitions based on oxidative processes.

Despite the extensive literature on GaAs oxidation and, more recently, syntheses devoted specifically to Ga_2O_3 NW formation, the structures produced here appear to be amongst if not the thinnest Ga_2O_3 wires fabricated. In initial studies, the intent of simply forming a passivation layer for GaAs was performed at temperatures hundreds of degrees below our process and in the presence of excess oxygen. Typically the synthesis procedures for intentionally growing Ga_2O_3 wires have resulted in diameters of tens to thousands of nanometers; these routes often employ a preponderance of gallium and/or oxygen. Our process differs from early passivation studies in the use of elevated temperature and lower oxygen content. It differs from most Ga_2O_3 NW studies, even those at comparable temperatures, in that we employ low oxygen content and a limited Ga supply. It is worth drawing explicit attention to these factors which may explain the absence of similar structures in the literature and may stimulate additional studies on ultra-sharp tips of Ga and other metal oxides.

The transmission electron microscopy (TEM) image (Fig. 2(e)) of sharp tip and X-ray diffraction pattern show evidence that the as-grown structures are single-crystal monoclinic Ga_2O_3. An ensemble of protrusions is visible on the tip. Similar NW decoration was observed by Shin et al. and was reportedly a defect-free Ga_2O_3 NW/nanocrystal homojunction.[30]

The schematic for the field emission measurement setup is shown in Figure 6(a). We performed the measurements in a high-vacuum chamber ($\sim 10^{-8}$ Torr). The sample was fixed onto an aluminum SEM sample holder that also functioned as the cathode contact while a polished stainless steel plate was used as an anode. The distance between the anode and the ultra-sharp tips, d, of the Ga_2O_3 nanorods was around 1 mm. The measured area was $\sim$76.5 mm^2.

Figure 6(b) shows the measured field emission J–E characteristic, along with its corresponding Fowler-Nordheim (FN) plot. To analyze the emission current, I_{FN}, we applied a modified version of the FN equation similar

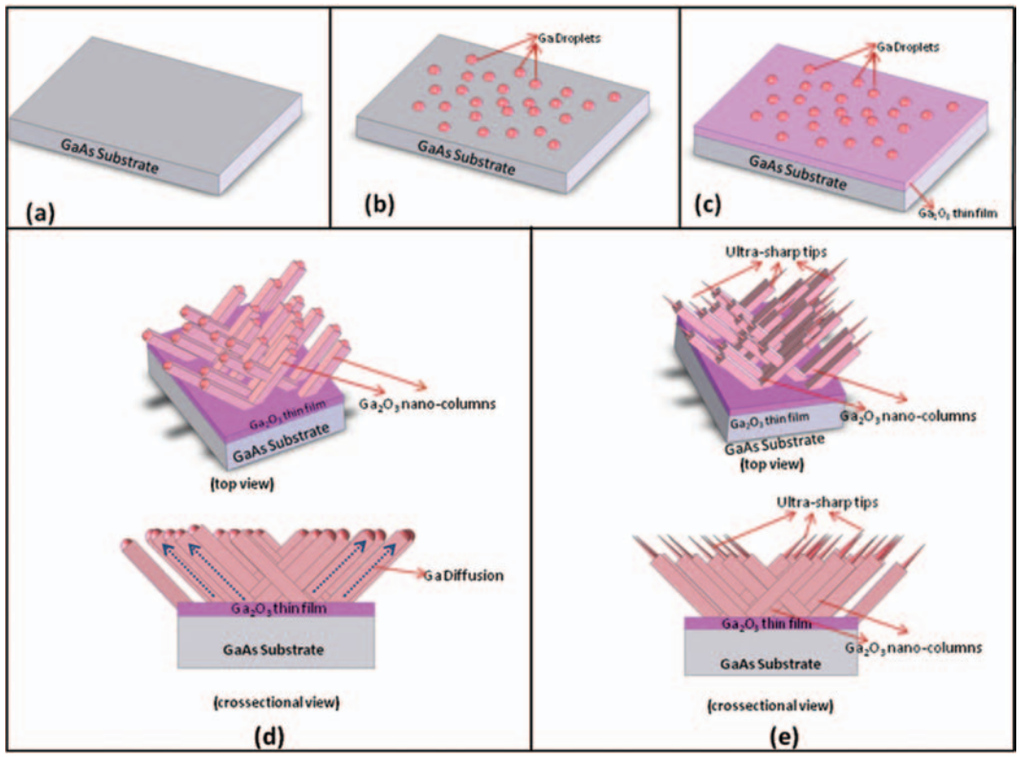

Fig. 4. Schematic representation of the growth process. (a) GaAs substrate. (b) At around the decomposition temperature (585 °C), the lattice structure begins to break down and preferential loss of arsenic (As) occurs from the GaAs surface. (c) With sufficient supply of oxygen in the ambient, Ga droplets on the surface tend to form a Ga_2O_3 thin film or (d) micro/nano Ga_2O_3 blocks. (e) When there is very little amount of metal Ga left on top of nano-micro Ga_2O_3 blocks, ultra-sharp tip growth takes place.

to earlier works.[31,32] In contrast to metals, field penetration into semiconductors can cause deformation of the conduction band. At high field strengths, the bottom of the conduction band will dip below the Fermi level, creating an electron pool at the surface.[31,33] The effective work function, as used in the FN formalism, will then be given by:

$$\phi_{\text{eff}} = \phi - \zeta E_{\text{loc}}^{4/5} \text{ eV}$$

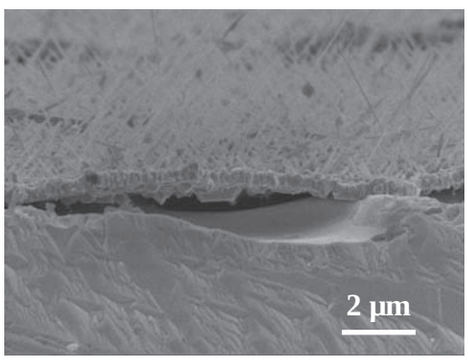

Fig. 5. Cross-sectional SEM image of GaAs Substrate with Ga_2O_3 thin film and nanorods anchored on it. The voids between micro-scale film on the substrate and the GaAs substrate are clearly discernable in the image.

where E_{loc} is the local field, ϕ is the semiconductor work function (4.15 eV for Ga_2O_3[34]), and the constant ζ is given by $\zeta = 4.5 \times 10^{-7} \varepsilon_r^{-2/5}$ $\text{eV}^{1/5}$ $\text{cm}^{4/5}$.

The resulting FN equation is

$$I_{\text{FN}} = A \cdot J_{\text{FN}} = A \frac{a}{t(y)^2} \frac{E^2}{\phi_{\text{eff}}} \exp\left[-b \frac{\phi_{\text{eff}}^{3/2}}{E} v(y)\right] \times \left[1 - \left(1 + \frac{2\kappa\zeta E^{4/5} \phi_{\text{eff}}^{1/2}}{E}\right) + \exp\left(\frac{2\kappa\zeta E^{4/5} \phi_{\text{eff}}^{1/2}}{E}\right)\right] \text{A} \cdot \text{cm}^{-2} \quad (1)$$

where A is the effective emission area, a and b are the universal FN constants, $\kappa = 5.16 \times 10^7$ $\text{eV}^{-1/2}$ cm^{-1}, and y is the image force barrier lowering factor given by

$$y = c \frac{F^{1/2}}{\phi_{\text{eff}}} \left(\frac{\varepsilon_r - 1}{\varepsilon_r + 1}\right)^{1/2} \quad (2)$$

where $c = 3.7947 \times 10^{-4}$ eV $\text{V}^{-1/2}$ $\text{cm}^{1/2}$, ε_r is the semiconductor dielectric constant (10.2 for Ga_2O_3[35]), and $t(y)$ and $v(y)$ are the correction functions (elliptical factors).[36] The slope of the FN curves in the linear regime, S, is proportional to $\phi_{\text{eff}}^{3/2}$,[33] and is given by:

$$S \equiv \partial \ln(I_{\text{FN}}/V^2)/\partial(1/V) \quad (3)$$

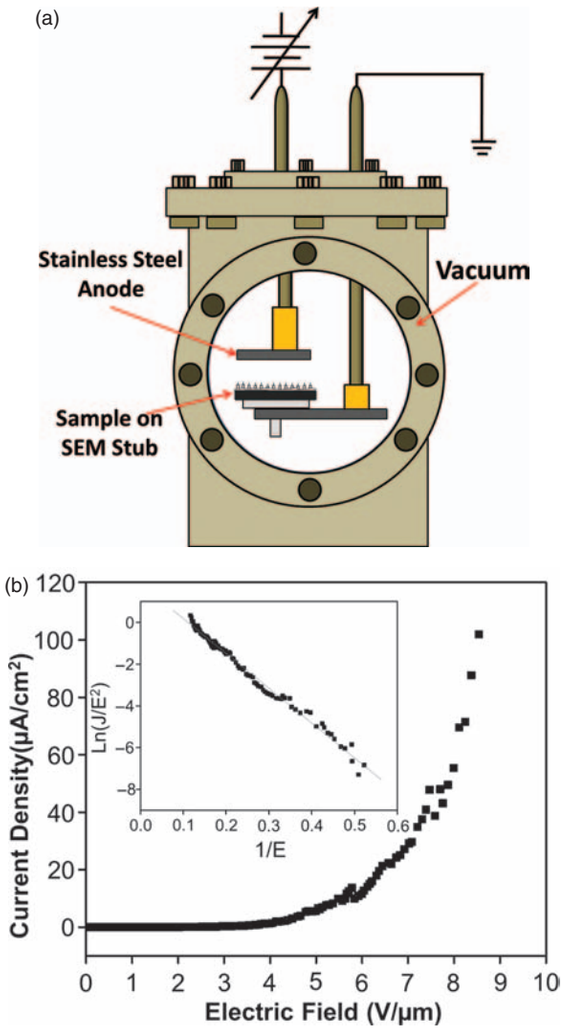

Fig. 6. (a) Schematic of the Field Emission measurement setup. (b) The emission current density from the Ga_2O_3 nanotips versus applied field (J–E). The turn-on field of 2.1 Vμm^{-1} and the threshold field of 5.6 Vμm^{-1} are obtained. The inset is the F–N plot, demonstrating a linear characteristic which is typical of field emission.

Equation (3) was solved numerically to find the field enhancement factor (FEF) for the nanowires defined as $\beta = E_{loc}/E_{app}$, where E_{loc} and E_{app} are the amplified local, and applied parallel-plate field strengths respectively, the latter given by $E_{app} = V/d$. An average value of $\beta \approx 3786$ was obtained from our measurements. The effective emission area, calculated using the auxiliary function $\Gamma(y)$ as proposed by Forbes,[36] was found to be $A \approx 2.31 \times 10^{-17}$ cm^2.

The turn-on field, which we designate to represent the electric field required to generate an emission current density of 10 μA cm^{-2}, was about 2.1 Vμm^{-1}. The threshold field which we designate to represent the electric field required to generate an emission current density of 10 mA cm^{-2} was about 5.6 Vμm^{-1}. It is important to note that the turn-on voltage of ~2.3 Vμm^{-1} is as low as reported from nanostructured diamond (3–5 Vμm^{-1})[37] or from highly-oriented single wall carbon nanotubes (0.7–3.9 Vμm^{-1}).[38] These excellent field emission characteristics make Ga_2O_3 nanorods a viable candidate for industrial field emission applications.

Table I. A comparison of the field emission parameters of various nano structures.

Nanostructures	Turn-on field (Vμm^{-1})	Threshold field (Vμm^{-1})
Ga_2O_3 Ultra-sharp tips	**2.1**	**5.6**
Carbon nanotubes[39]	0.75	1.6
CN_X nanotubes[40]	2–3	5.5
ZnO nanotowers[15]	4.5	7.2
AlN nanotips[41]	4.7	10.6
GaAs nanowires[42]	2	6.5
GaN nanobelts[43]	1.3	2.3
NiO nanorods[44]	11.5	6.5
ZnO agavelike NWs[45]	2.4	4.3
Cactus-like Ga_2O_3Nanostructures[15]	12.6	23.2
Ga_2O_3–C nanocables[19]	7.73	8.45
Quasy-aligned Ga_2O_3 nanowires[20]	6.2	N/A
Tapered carbon nanotubes[46]	3.2	4.2
In_2O_3 nanowire-decorated Ga_2O_3 nanobelt heterostructures[47]	1.31	N/A
Boron nanowire arrays[48]	5.1	11.1

Table I details the comparison between some of the published data on the turn-on field and the threshold field with our Ga_2O_3 ultra-sharp nanorods. With a turn-on field of 2.1 Vμm^{-1}, a threshold electric field of 5.6 Vμm^{-1}, and a geometrical field enhancement factor of 3786, Ga_2O_3 ultra-sharp nanorods are better than several other commonly used nanostructures and are comparable to nanostructured diamond and highly oriented single wall carbon nanotubes.

4. CONCLUSION

In conclusion we have synthesized β-Ga_2O_3 nano-columns with ultra-sharp tips via a simple thermal CVD technique. In this growth process, the Ga source comes from the GaAs substrate. Nano-columns are formed by thermal oxidation of coalesced metal Ga droplets. Upon consumption of the droplet, ultra-sharp tips form. Field emission properties of the structures were investigated and the structures were found to exhibit excellent characteristics with a low turn-on field of 2.1 Vμm^{-1}, a low threshold electric field of 5.6 Vμm^{-1}. Using a modified version of the FN formalism, the high field enhancement factor (β) of the nanostructures was estimated to be 3786. The growth dynamics of ultra-sharp tip formation will benefit from further investigation; however, the synthetic route presented here already shows the capability of forming Ga_2O_3 NWs with diameters $\leq$10 nm. Additionally, the measured characteristics show promise for field emission device applications.

Acknowledgment: The work reported herein was partially supported by a University of California CITRIS research grant, NSF grant #0547679 and an Army Research Office (ARO) research grant 55176-EL-DRP.

References and Notes

1. S. J. Kang, C. Kocabas, T. Ozel, M. Shim, N. Pimparkar, M. A. Alam, S. V. Rotkin, and J. A. Rogers, *Nat. Nanotechnol.* 2, 230 (**2007**).
2. T. Kuykendall, P. J. Pauzauskie, Y. Zhang, J. Goldberger, D. Sirbuly, J. Denlinger, and P. Yang, *Nat. Mater.* 3, 524 (**2004**).
3. D. Q. Zhang, R. R. Wang, M. C. Wen, D. Weng, X. Cui, J. Sun, H. X. Li, and Y. F. Lu, *J. Am. Chem. Soc.* 134, 14283 (**2012**).
4. N. Du, H. Zhang, B. D. Chen, X. Y. Ma, Z. H. Liu, J. B. Wu, and D. R. Yang, *Adv. Mater.* 19, 1641 (**2007**).
5. S. M. Peng, Y. K. Su, and L. W. Ji, *Microelectron Eng.* 100, 16 (**2012**).
6. H. Guo, R. Mao, X. J. Yang, S. X. Wang, and J. Chen, *J. Power Sources* 219, 280 (**2012**).
7. L. C. Tien, C. C. Tseng, and C. H. Ho, *J. Electron Mater.* 41, 3056 (**2012**).
8. I. Lopez, E. Nogales, P. Hidalgo, B. Mendez, and J. Piqueras, *Physica Status Solidi a—Applications and Materials Science* 209, 113 (**2012**).
9. H. Zoltan, M. Jozsef, K. Gabor, R. Ferenc, D. Peter, C. H. Roy, and J. M. Kuperberg, *J. Appl. Phys.* 86, 3792 (**1999**).
10. Y. W. Wang, C. H. Liang, G. Z. Wang, T. Gao, S. X. Wang, J. C. Fan, and L. D. Zhang, *J. Mater. Sci. Lett.* 20, 1687 (**2001**).
11. Z. Liu, T. Yamazaki, Y. Shen, T. Kikuta, N. Nakatani, and Y. Li, *Sens. Actuators B* 129, 666 (**2008**).
12. W. Tian, C. Y. Zhi, T. Y. Zhai, S. M. Chen, X. Wang, M. Y. Liao, D. Golberg, and Y. Bando, *J. Mater. Chem.* 22, 17984 (**2012**).
13. Y. C. Choi, W. S. Kim, Y. S. Park, S. M. Lee, D. J. Bae, Y. H. Lee, G. S. Park, W. B. Choi, N. S. Lee, and J. M. Kim, *Adv. Mater.* 12, 746 (**2000**).
14. J. Q. Hu, Q. Li, X. M. Meng, C. S. Lee, and S. T. Lee, *J. Phys. Chem. B* 106, 9536 (**2002**).
15. C. Cao, Z. Chen, X. An, and H. Zhu, *J. Phys. Chem. C* 112, 95 (**2008**).
16. J. P. Liu, X. T. Huang, Y. Y. Li, X. X. Ji, Z. K. Li, X. He, and F. L. Sun, *J. Phys. Chem. C* 111, 4990 (**2007**).
17. I. Brodie and C. A. Spindt, Vacuum microelectronics, Advances in Electronics and Electron Physics, edited by P. W. Hawkes, Elsevier Inc. (**1992**), Vol. 83, p. 1.
18. C. A. Spindt, C. E. Holland, A. Rosengreen, and I. A. B. I. Brodie, *IEEE Transactions on Electron Devices* 38, 2355 (**1991**).
19. J. Zhan, Y. Bando, J. Hu, Y. Li, and D. Golberg, *Chem. Mater.* 16, 5158 (**2004**).
20. Y. Huang, Z. Wang, Q. Wang, C. Gu, C. Tang, Y. Bando, and D. Golberg, *The Journal of Physical Chemistry C* 113, 1980 (**2009**).
21. K. C. Lo, H. P. Ho, K. Y. Fu, P. K. Chu, K. F. Li, and K. W. Cheah, *J. Appl. Phys.* 95, 8178 (**2004**).
22. K. Shorlin and M. Zinke-Allmang, *Surf. Sci.* 601, 2438 (**2007**).
23. T. D. Lowes and M. Zinke-Allmang, *J. Appl. Phys.* 73, 4937 (**1993**).
24. M. Zinke-Allmang, L. C. Feldman, and W. Vansaarloos, *Phys. Rev. Lett.* 68, 2358 (**1992**).
25. T. Mano, T. Kuroda, S. Sanguinetti, T. Ochiai, T. Tateno, J. Kim, T. Noda, M. Kawabe, K. Sakoda, G. Kido, and N. Koguchi, *Nano Lett.* 5, 425 (**2005**).
26. C. Heyn, A. Stemmann, A. Schramm, H. Welsch, W. Hansen, and A. Nemcsics, *Phys. Rev. B* 76 (**2007**).
27. J. Tersoff, D. E. Jesson, and W. X. Tang, *Science* 324, 236 (**2009**).
28. O. R. Monteiro and J. W. Evans, *J. Vac. Sci. Technol. A* 7, 49 (**1989**).
29. S. Sharma and M. K. Sunkara, *J. Am. Chem. Soc.* 124, 12288 (**2002**).
30. T. I. Shin, H. J. Lee, W. Y. Song, S. W. Kim, M. H. Park, C. W. Yang, and D. H. Yoon, *Nanotechnology* 18, 345305 (**2007**).
31. R. Stratton, *Proceedings of the Physical Society of London Section B* 68, 746 (**1955**).
32. R. Banan-Sadeghian, S. Badilescu, Y. Djaoued, S. Balaji, V. V. Truong, and M. Kahrizi, *IEEE Electron Device Letters* 29, 312 (**2008**).
33. A. J. Melmed and R. Gomer, *J. Chem. Phys.* 34, 1802 (**1961**).
34. J. Robertson and B. Falabretti, *Materials Science and Engineering B-Solid State Materials for Advanced Technology* 135, 267 (**2006**).
35. M. Passlack, M. Hong, E. F. Schubert, J. P. Mannaerts, W. S. Hobson, N. Moriya, J. Lopata, and G. J. Zydzik, *Compound Semiconductors* 1994, 597 (**1995**).
36. R. G. Forbes, *J. Vac. Sci. Technol. B* 17, 526 (**1999**).
37. D. He, L. Shao, W. Gong, E. Xie, K. Xu, and G. Chen, *Diam. Relat. Mater.* 9, 1600 (**2000**).
38. C. M. Yeh, M. Y. Chen, J. Hwang, J. Y. Gan, and C. S. Kou, *Nanotechnology* 5930 (**2006**).
39. A. M. Rao, D. Jacques, R. C. Haddon, W. Zhu, C. Bower, and S. Jin, *Appl. Phys. Lett.* 76, 3813 (**2000**).
40. D. Golberg, P. S. Dorozhkin, Y. Bando, Z. C. Dong, C. C. Tang, Y. Uemura, N. Grobert, M. Reyes-Reyes, H. Terrones, and M. Terrones, *Applied Physics A: Materials Science and Processing* 76, 499 (**2003**).
41. Y. Tang, H. Cong, Z. Chen, and H. Cheng, *Appl. Phys. Lett.* 86, 233104 (**2005**).
42. C. Y. Zhi, X. D. Bai, and E. G. Wang, *Appl. Phys. Lett.* 86, 213108 (**2005**).
43. T. Yamashita, S. Hasegawa, S. Nishida, M. Ishimaru, Y. Hirotsu, and H. Asahi, *Appl. Phys. Lett.* 86, 082109 (**2005**).
44. Z. Zhang, Y. Zhao, and M. Zhu, *Appl. Phys. Lett.* 88, 033101 (**2006**).
45. Y. H. Yang, B. Wang, N. S. Xu, and G. W. Yang, *Appl. Phys. Lett.* 89, 043108 (**2006**).
46. W. H. Lin and Y. Y. Li, *Diam. Relat. Mater.* 22, 124 (**2012**).
47. J. Lin, Y. Huang, Y. Bando, C. C. Tang, C. Li, and D. Golberg, *ACS Nano* 4, 2452 (**2010**).
48. F. Liu, J. F. Tian, L. H. Bao, T. Z. Yang, C. M. Shen, X. Y. Lai, Z. M. Xiao, W. G. Xie, S. Z. Deng, J. Chen, J. C. She, N. S. Xu, and H. J. Gao, *Adv. Mater.* 20, 2609 (**2008**).

ARTICLE